Appl. Phys. A 89, 667–671 (2007)
DOI: 10.1007/s00339-007-4199-y

Applied Physics A
Materials Science & Processing

WALLACE C.H. CHOY[1,✉]
J.H. NIU[1,2]
XUE-WEN CHEN[1,3]
W.L. LI[2]
P.C. CHUI[1]

Effects of carrier barrier on voltage controllable color tunable OLEDs

[1] Department of Electrical and Electronic Engineering, University of Hong Kong, Pokfulam Road, Hong Kong, P.R. China
[2] Changchun Institute of Optics, Fine Mechanics and Physics, Chinese Academy of Sciences, Changchun 130033, P.R. China
[3] Centre for Optical and Electromagnetic Research, Zhejiang University, Hangzhou 310058, P.R. China

Received: 16 February 2007/Accepted: 13 June 2007
Published online: 28 July 2007 •

ABSTRACT The effects of the carrier blocking layer on the emission color of the color tunable organic light emitting devices (OLEDs) have been investigated. Color tuning is controlled by the applied voltage. Both the experimental and theoretical results show that inserting a hole blocking layer between two adjacent emission layers will make the color tunable region move toward the wide bandgap emission layer of blue color in our case. By replacing the hole blocking layer with an electron blocking layer, the color tunable region will shift toward the small bandgap emission layer of red. Besides shifting the tunable region toward the pure spectral color, the introduction of the carrier blocking layer can extend the color tunable range.

PACS 78.20.Bh; 78.45.+h; 78.55.Kz; 78.60.Fi; 81.05.Lg; 85.60.Jb

1 Introduction

With the interesting features of for instance light weight, thin structure thickness and flexible configuration, organic light emitting devices (OLEDs) are useful devices for flat panel displays, illustration and signaling. Voltage-controlled color tunable OLED is a potential candidate for the use of full-color operation without the complicated structures common to other types of devices using red, green and blue pixels. Color tunable OLEDs from both small molecules [1–3] and a blend of polymers [4–6] have been reported. In the color tunable OLEDs, organic materials (small molecules and polymers) with different spectral energy distributions have been used in a single device unit and response for emitting the tunable color obtained by varying the applied voltage. Generally, a higher voltage results in more emission from the higher bandgap organic materials, which emits radiation toward the blue region of the spectrum, while also resulting in higher overall brightness due to increased current injection into the device. Although color tuning, such as from orange to white [4] has been demonstrated, the incomplete quenching of low band-gap material prohibits the tuning into pure blue. Therefore, it is desirable to have a device which can have complete quenching of low band-gap material thus enabling tuning into the primary color.

In this report, we will theoretically and experimentally investigate the effects of carrier barriers (including hole and electron blocking layers) of the device structure on the emission color of the color-tunable OLEDs. The color tuning is obtained by changing the applied bias. In our study, a layer of carrier barrier is introduced between two intentionally emissive layers for improving the spectral color and extending the tunable range, while the carrier blocking layers are generally used to confine the emission region for a strict color emission without the color tunability. Our results show that, the introduction of the carrier barrier with suitable thickness and location in the device structure can not only moves the whole color tuning route toward the pure color but also extends the color tuning range.

2 Experiment and theoretical model

2.1 *Experiment*

The indium-tin-oxide (ITO) substrates with a size of $25 \times 25\,\mathrm{mm}^2$ and resistivity of $80\,\Omega$/square were cleaned prior to loading into the evaporation chamber through scrubbing by detergent and soaking into de-ionized (DI) water for 10 min in each step. The evaporation chamber is operated at $\sim 10^{-7}$ Torr. The substrates were then immersed into ultrasonic bath of DI water, ethanol and acetone for 20 min for each solvent. The solvent cleaned ITO substrates were further treated in UV ozone for 20 min. The organic materials used in this study were aluminum tris(8-hydroxyquinoline) Alq_3 acted as an electron transport layer, N,N'-bis(1-naphthyl)-N,N'-diphenyl-1,1′-biphenyl-4,4′-diamine (NPD) as a hole transport layer, 2-methyl-9,10-dis-2-naphthyldanthracene (MADN) as the blue emitter and host, 2,9-Dimethyl-4,7-diphenyl-1,10-phenanhroline (BCP) and 4,4′,4″-Tris (*N*-3-methylphenyl-*N*-phenyl-amino) triphenylamine (*m*-MDATA) as the electron (EBL) and hole (HBL) blocking layers respectively, 4-(dicyano-methylene)-2-methyl-6-(*p*-dimethyl aminostyryl)-4H-pyran (DCM1) as the red dye, copper phthalocyanine (CuPc) for stabilizing the ITO surface and LiF as the electron injection layer (EIL). The materials were purified by gradient sublimation prior

✉ Fax: 852-2559-8738, E-mail: chchoy@eee.hku.hk

to thin-film coating however DCM1 was used without further purification. The deposition rate for CuPc, Alq_3, NPD, MADN, BCP, *m*-MDATA was typically 1.0–2.0 Å/s. The deposition rates of LiF and Al were 0.1 Å/s and 10–15 Å/s, respectively. Film thickness was monitored in situ using the quartz crystal monitor and ex situ by a stylus profilometer (Tencor α-step 500).

To investigate the contributions of the EBL and HBL to the emission color of the tunable OLEDs, three OLED structures containing various carrier blocking layers as shown in Fig. 1 have been prepared.

Device A: ITO/ CuPc (15 nm)/ NPD (70 nm)/ MADN (30 nm)/ MADN:DCM1(2%) (10 nm)/ BCP (7 nm)/ Alq_3 (25 nm)/ LiF (0.5 nm)/ Al.

Device B: ITO/ CuPc (15 nm)/ NPD (70 nm)/ MADN (30–*x* nm)/ HBL (*x* nm)/ MADN:DCM1(2%) (10 nm)/ BCP (7 nm)/Alq_3 (25 nm)/ LiF (0.5 nm)/ Al.

Device C: ITO/ CuPc (15 nm)/ NPD (70 nm)/ MADN (30–*x* nm)/ EBL (*x* nm)/ MADN:DCM1(2%) (10 nm)/ BCP (7 nm)/Alq_3 (25 nm)/ LiF (0.5 nm)/ Al.

The devices were characterized in room ambient without encapsulation. The current density–voltage–luminance (*J*–*V*–*L*) characteristics of the devices were measured with an International Light IL1400A photometer and a Keithley source meter 2400.

2.2 *Theoretical model*

In order to understanding the color tuning spectrum of the devices, the light emission of multilayered OLED structures as shown in Fig. 2 is rigorously modeled through a classical electromagnetic approach with an emitting layer sandwiched between two stacks of films (*M* layers above and *N* layers below) taking into account the Purcell effect. The vertical electric dipole (VED) and horizontal electric dipole (HED) are located in the recombination zone with distances Z_+ and Z_- from the layer with notation of 1 and -1, respectively. The two stacks of films can be considered as two effective interfaces characterized by the total reflection and transmission coefficients $r^{\mathrm{TM/TE}}_{e,M/-N}$ and $t^{\mathrm{TM/TE}}_{e,M/-N}$ as shown in Fig. 2. Details of the expression can refer to [7]. The total radiation power, normalized by the radiation power of the dipole in an infinite medium ε_e, can be expressed as [8]

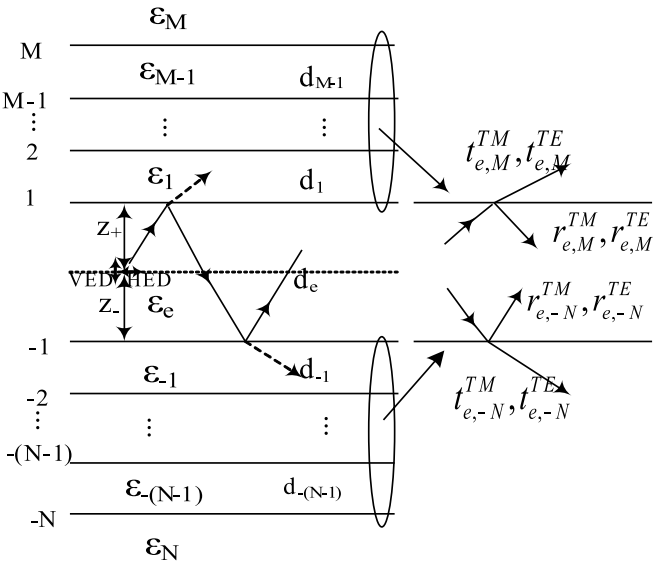

FIGURE 2 A planar multilayer OLED consisting of an emitting layer and two film stacks with relative permittivity and thickness of (ε_i, d_i) $(i = -N, ..., -1, e, 1, ..., M)$ for each layer. VED and HED are located in the emitting layer with distances Z_+ and Z_- from the layer with notation of 1 and -1. The simplified structure described by $r^{\mathrm{TM/TE}}_{e,M/-N}$ and $t^{\mathrm{TM/TE}}_{e,M/-N}$ is shown in the right-hand side

$$F_{\mathrm{V}} = \int_0^{\infty} \Re\left[\frac{3k_\varrho^2\left(1+r^{\mathrm{TM}}_{e,M}\,\mathrm{e}^{2jk_{z,e}z_+}\right)\left(1+r^{\mathrm{TM}}_{e,-N}\,\mathrm{e}^{2jk_{z,e}z_-}\right)}{4k_{z,e}k_e^3\left(1-r^{\mathrm{TM}}_{e,M}r^{\mathrm{TM}}_{e,-N}\,\mathrm{e}^{2jk_{z,e}d_e}\right)}\right]\mathrm{d}\left(k_\varrho^2\right) \tag{1}$$

$$F_{\mathrm{H}} = \int_0^{\infty} \Re\left[\frac{3k_{z,e}\left(1-r^{\mathrm{TM}}_{e,M}\,\mathrm{e}^{2jk_{z,e}z_+}\right)\left(1-r^{\mathrm{TM}}_{e,-N}\,\mathrm{e}^{2jk_{z,e}z_-}\right)}{8k_e^3\left(1-r^{\mathrm{TM}}_{e,M}r^{\mathrm{TM}}_{e,-N}\,\mathrm{e}^{2jk_{z,e}d_e}\right)}\right]\mathrm{d}\left(k_\varrho^2\right)$$
$$+\int_0^{\infty} \Re\left[\frac{3\left(1+r^{\mathrm{TE}}_{e,M}\,\mathrm{e}^{2jk_{z,e}z_+}\right)\left(1+r^{\mathrm{TE}}_{e,-N}\,\mathrm{e}^{2jk_{z,e}z_-}\right)}{8k_ek_{z,e}\left(1-r^{\mathrm{TE}}_{e,M}r^{\mathrm{TE}}_{e,-N}\,\mathrm{e}^{2jk_{z,e}d_e}\right)}\right]\mathrm{d}\left(k_\varrho^2\right) \tag{2}$$

for VED and HED, respectively. $\Re[\cdot]$ stands for the real part of $[\cdot]$. k_ϱ and $k_{z,e}$ are the radial and z component of the wave vector in cylindrical coordinates. $k_{z,i}$ in the ith layer $(i = M, ..., 1, e, -1, ..., -N)$ is given by

$$k_{z,i} = \left(k_0^2\varepsilon_i - k_\varrho^2\right)^{1/2}, \tag{3}$$

where k_0 is the wave number in vacuum. We define $k_{z,i}$ in the first quadrant of the complex plane to ensure the radiation condition at infinity. The normalized power transmitted to region *M* is given by [8]

$$U_{\mathrm{V}} = \int_0^{\infty} \frac{3\varepsilon_e k_\varrho^2\left|1+r^{\mathrm{TM}}_{e,M}\,\mathrm{e}^{2jk_{z,e}z_+}\right|^2\left|t^{\mathrm{TM}}_{e,M}\right|^2\Re\left[\frac{k_{z,M}}{\varepsilon_M}\right]\mathrm{e}^{-2\Im(k_{z,e})z_+}}{8k_e^3\left|k_{z,e}^2\right|\left|1-r^{\mathrm{TM}}_{e,M}r^{\mathrm{TM}}_{e,-N}\,\mathrm{e}^{2jk_{z,e}d_e}\right|^2}\mathrm{d}\left(k_\varrho^2\right), \tag{4}$$

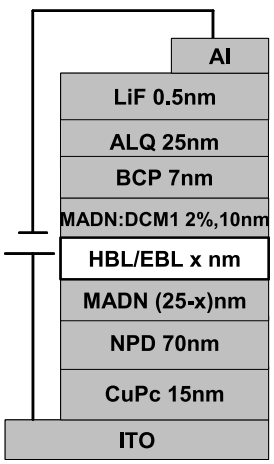

FIGURE 1 Device configuration: ITO/ CuPc (15 nm)/ NPD (70 nm)/ MADN (30–*x* nm)/ EBL or HBL (*x* nm)/MADN:DCM1 (2%) (10 nm)/ BCP (7 nm)/Alq_3 (25 nm)/LiF (0.5 nm)/Al

$$U_{\mathrm{H}} = \int_0^{\infty} \frac{3\varepsilon_e \left|1 - r_{e,M}^{\mathrm{TM}} \mathrm{e}^{2jk_{z,e}z_+}\right|^2 \left|t_{e,M}^{\mathrm{TM}}\right|^2 \Re\left[\frac{k_{z,M}}{\varepsilon_M}\right] \mathrm{e}^{-2\Im(k_{z,e})z_+}}{16k_e^3 \left|1 - r_{e,M}^{\mathrm{TM}} r_{e,-N}^{\mathrm{TM}} \mathrm{e}^{2jk_{z,e}d_e}\right|^2} \mathrm{d}\left(k_\varrho^2\right) + \int_0^{\infty} \frac{3\left|1 + r_{e,M}^{\mathrm{TE}} \mathrm{e}^{2jk_{z,e}z_+}\right|^2 \left|t_{e,M}^{\mathrm{TM}}\right|^2 \Re\left[k_{z,M}\right] \mathrm{e}^{-2\Im(k_{z,e})z_+}}{16k_e \left|k_{z,e}^2\right| \left|1 - r_{e,M}^{\mathrm{TE}} r_{e,-N}^{\mathrm{TE}} \mathrm{e}^{2jk_{z,e}d_e}\right|^2} \mathrm{d}\left(k_\varrho^2\right) \tag{5}$$

for VED and HED, respectively. Here $\Im(\cdot)$ stands for the imaginary part of $(\cdot)$. For a randomly oriented dipole with equal probability for all directions in space, we have

$$F_{\mathrm{R}} = \frac{1}{3}F_{\mathrm{V}} + \frac{2}{3}F_{\mathrm{H}} = \int_0^{\infty} \Re\left[f_{\mathrm{R}}\left(k_\varrho\right)\right] \mathrm{d}k_\varrho\,, \tag{6}$$

$$U_{\mathrm{R}} = \frac{1}{3}U_{\mathrm{V}} + \frac{2}{3}U_{\mathrm{H}}\,, \tag{7}$$

where $f_{\mathrm{R}}\left(k_\varrho\right)$ can be readily obtained by comparing (6) with (1) and (2). By rewriting the transmitted power as

$$F_{\mathrm{R}} = \frac{1}{3}F_{\mathrm{V}} + \frac{2}{3}F_{\mathrm{H}} = \int_0^{\infty} \Re\left[f_{\mathrm{R}}\left(k_\varrho\right)\right] \mathrm{d}k_\varrho \tag{8}$$

$$U_{\mathrm{R}} = \int_0^{\infty} u_{\mathrm{R}}\left(k_\varrho\right) \mathrm{d}\left(k_\varrho^2\right) \tag{9}$$

and assuming ε_M is real, the normalized power density P at a viewing angle α in region M can be obtained as

$$P(\alpha) = \varepsilon_M k_0^2 \cos\alpha u_{\mathrm{R}}\left(k_0 \varepsilon_M^{1/2} \sin\alpha\right)/\pi\,. \tag{10}$$

In our model, a comprehensive consideration of Fabry–Pérot effect [9] of weak microcavity OLEDs, the nonradiative losses due to the metal electrode and other materials used in the structure as well as the effects of thick glass substrate have been taken into account which have been ignored by others [10–12]. Details of the numerical treatment can refer to [7]. The refractive indices for organic materials, ITO and glass are assumed to be 1.77, $2.06 + 0.005\mathrm{i}$ and 1.5, respectively, unless specified. The complex permittivity of aluminum at wavelength 500 nm is taken from [13]. In modeling the emission spectrum, the electron and hole recombination location for the red color emission is considered at the layer of MADN:DCM1 and near to the interface between MADN:DCM1 and the carrier blocking layer. For the blue emission, the recombination location is considered at the layer of MADN and near to the interface between MADN and the carrier blocking layer. With the strength of the blue and red emission at various biases obtained from the experiment, their ratio is used for modeling the emission spectrum as shown in Figs. 5b and 6b.

3 Results and discussions

In order to achieve voltage controllable color tunability, two emission layers of MADN and MADN:DCM1 (2%) with emission color of blue and red respectively are utilized in device A. At a low bias voltage of 9 V, a dominant red emission from DCM1 is obtained. When the bias voltage increases, the red emission reduces and the blue emission from MADN increases. Generally, the change of the emission color can be explained by the extension of the exciton recombination region and the shift of the recombination region [2, 3]. From our results as shown in Fig. 3a, the redistribution of the exciton distribution in the recombination region should be used to explain the color tuning. It is because the photoluminescent (PL) spectrum of MADN:DCM1 (2%) (not shown in this article) is merely from DCM1. However, the electroluminescence (EL) spectrum of device A at low bias consists of the dominant peak of DCM1 and a satellite peak of MADN. Therefore, the excitons distribute in both layers of MADN:DCM1 (2%) and MADN, but are dominant at the former. When the voltage increases to 17 V, the excitons dominantly distribute in MADN and, thus, a strong emission from MADN with a weak DCM1 emission is obtained. As a result, a tunable OLED changing from dim red to dim blue has been obtained as shown in the CIE chromaticity diagram of Fig. 3b.

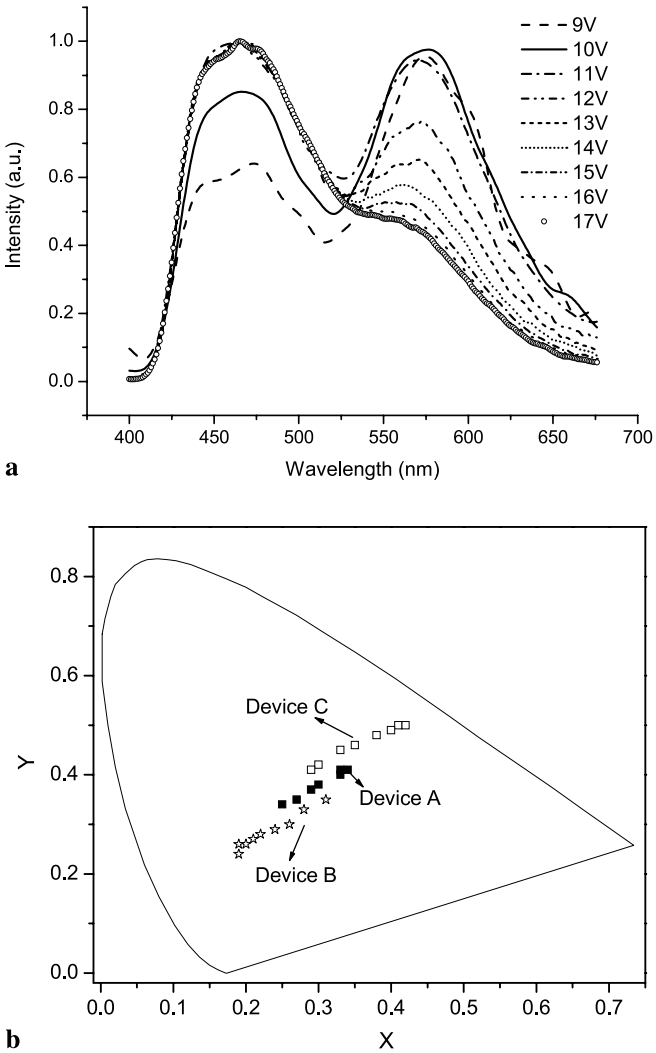

FIGURE 3 (**a**) The EL spectra of device A, (**b**) the CIE chromaticity diagram

In order to improve the color tunable range and purity, a carrier blocking layer is inserted between the two emis-

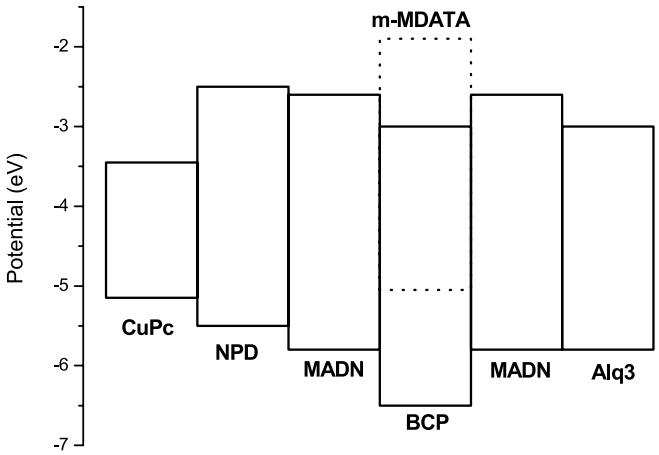

FIGURE 4 An energy diagram of the HOMO and LUMO positions of the various organic materials for device A to C

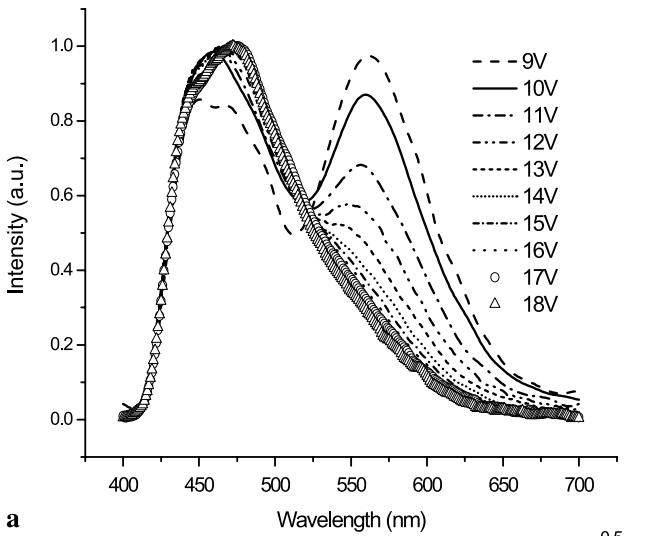

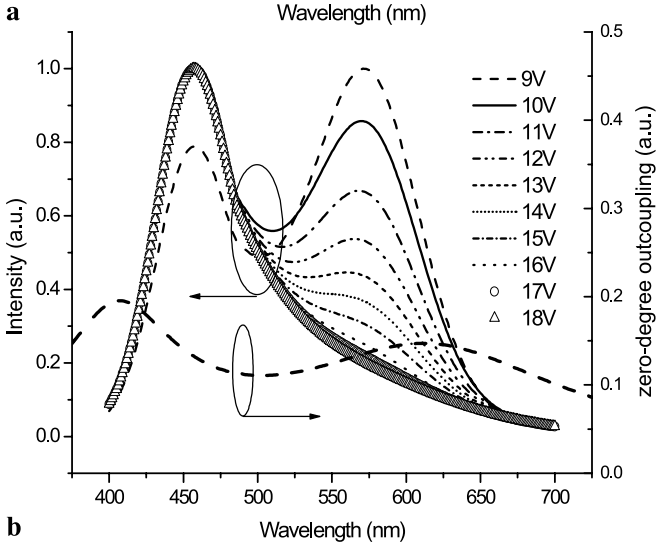

FIGURE 5 (**a**) The EL spectra of device B with 5 nm BCP as the HBL, (**b**) the modeled EL spectra and the out-coupling efficiency normal to the device of device B

sion layers of MADN:DCM1 (2%) and MADN. For device B, BCP is used as HBL as shown in Fig. 4. With a suitable thickness of 5 nm, the red emission of satellite peak at wavelength of 565 nm can be completely quenched at high bias of

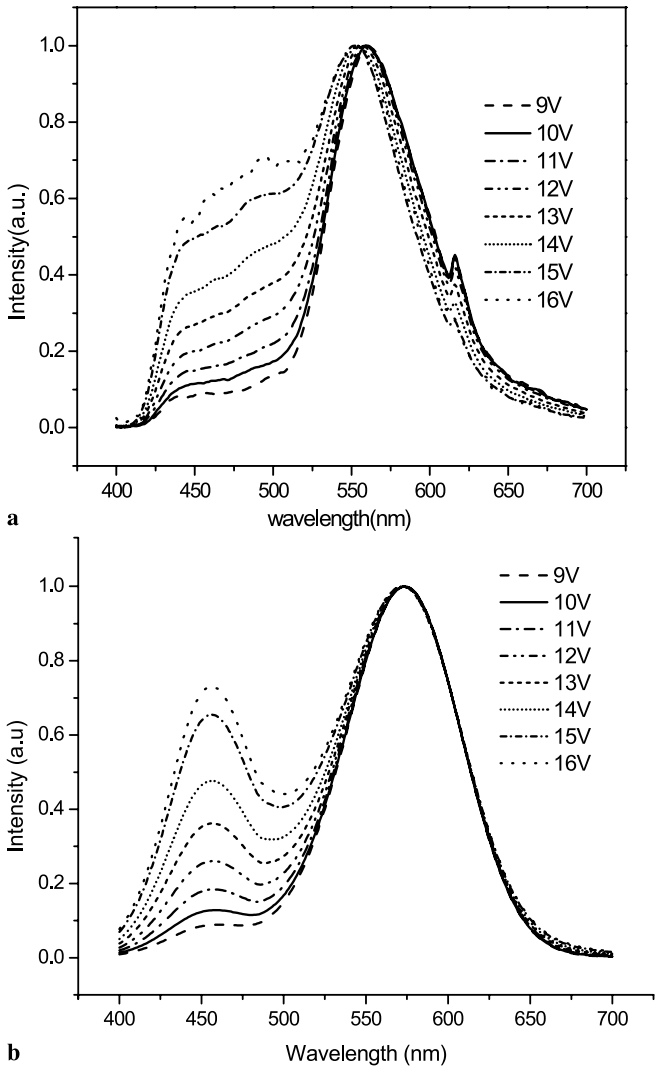

FIGURE 6 (**a**) The EL spectra of device C with 5 nm *m*-MDATA as the EBL, (**b**) the modeled EL spectra of device C

17 V. At that time, only the blue emission from MADN is obtained as shown in Fig. 5a. Modeling has been conducted for device B with 5 nm of BCP as the HBL and the result is shown in Fig. 5b. The theoretical result shows very good agreement to the experiment as compared to Fig. 5a. By comparing with the PL spectrum of NADN thin film, the microcavity effect on the EL spectrum is not significant and the peak of the emission peak only shifts from 450 nm from PL to 458 nm in device. The spectrum of outcoupling efficiency normal to the device (Fig. 5b) varies mildly and the peaks of the outcoupling efficiency are board, i.e., the microcavity effect is weak. Otherwise, with a strong microcavity effect, the full width half maximum of the emission spectra will significantly narrow down with large change in intensity.

To evaluate the contribution of red color emission of DCM1 in the device emission, the color fraction defined in (10) is plotted in Fig. 7.

$$\text{Color fraction} = \text{DCM1 emission/overall device emission}\,. \tag{11}$$

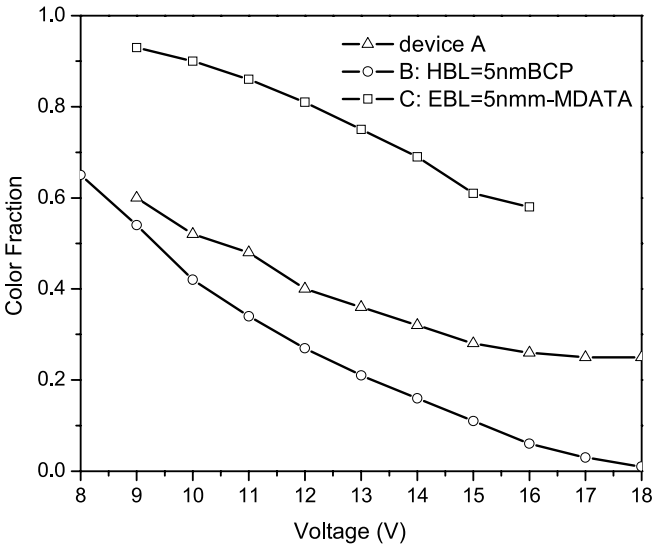

FIGURE 7 The color fraction of EL spectra of device A, B and C

One can see that when 5 nm of BCP is inserted between the two emission layers, the color fraction will reach zero at bias of 18 V, i.e., the EL emission is merely from MADN. This can be explained by the low highest-occupied-molecular orbital (HOMO) of BCP at -6.5 eV, which prevents the injection of holes from MADN with HOMO level of -5.8 eV to MADN:DCM1 (2%). Meanwhile, the low lowest-unoccupied molecular orbital (LUMO) of BCP at -3 eV does not block the electron injection into MADN. Therefore, when bias voltage is high enough, only the emission from MADN can be found. Consequently, as compared with device A, the BCP layer will make the color tuning region move towards blue and extend the emission range as shown in Fig. 3b.

By replacing the HBL with an EBL of *m*-MDATA with a suitable thickness of 5 nm, device C shows the color tuning as shown in Fig. 6a. Since LUMO of *m*-MDATA at -1.9 eV is high and blocks the electron injection to MADN layer, the emission is primarily from DCM1 at low bias voltage of 9 V. The experimental results are similar to those obtained from the model as shown in Fig. 6b. Due to the weak microcavity effect as discussed previously, the peak at 565 nm derives from that of DCM1 at about 590 nm. Consequently, with *m*-MDATA EBL, the color tunable region shifts toward the pure spectral color with a better color purity at low bias as shown in Fig. 3b. Even though the emission is slightly deviated from typical DCM1 emission, and the color fraction cannot reach unity as shown in Fig. 7, the overall tunable range is still larger than that of device A as shown in Fig. 3b. It should be noted that the color tuning route of all devices A, B and C are generally straight line. This implies that there is not unexpected emission origins generated by inserting the carrier blocking layer to the tunable OLEDs such as exciplex [2].

4 Conclusions

The effects of electron and hole blocking layers on the color emission of voltage controlled color tunable OLEDs have been experimentally and theoretically investigated. The theoretical results show good agreement with the experimental ones. By inserting HBL between two emission layers response for the color tuning route, the tuning region can be moved towards the high bandgap organic material of blue. Meanwhile, the EBL can shift the tuning region towards the low bandgap organic material of red. Besides moving the tuning region toward the pure spectral color, the voltage-controllable tunable range can be extended by introducing either EBL or HBL.

ACKNOWLEDGEMENTS We would like to acknowledge the support of UDF grant, the strategic research grant in organic optoelectronics of the University of Hong Kong and the grant (#14300.324.01) from the Research Grant Council of the Hong Kong Special Administrative Region, China.

REFERENCES

1 J. Kalinowski, P. Di Marco, M. Cocchi, N. Camaioni, J. Duff, Appl. Phys. Lett. **68**, 2317 (1996)
2 C.J. Liang, W.C.H. Choy, Appl. Phys. Lett. **89**, 251 108-1 (2006)
3 M. Yoshida, A. Fujii, Y. Ohmori, K. Yoshino, Appl. Phys. Lett. **69**, 734 (1996)
4 M. Granstrom, O. Inganas, Appl. Phys. Lett. **68**, 147 (1996)
5 B.O. Dabbousi, M.G. Bawendi, O. Onitsuka, M.F. Rubner, Appl. Phys. Lett. **66**, 1316 (1995)
6 C.C. Huang, H.F. Meng, G.K. Ho, C.H. Chen, C.S. Hsu, J.H. Huang, S.F. Horng, B.X. Chen, L.C. Chen, Appl. Phys. Lett. **84**, 1195 (2004)
7 X.W. Chen, W.C.H. Choy, S. He, IEEE J. Display Technol. **3**, 110 (2007)
8 K. Neyts, J. Opt. Soc. Am. A **15**, 962 (1998)
9 W.C.H. Choy, E.H. Li, IEEE J. Quantum Electron. **QE-33**, 382 (1997)
10 O.H. Crawford, J. Chem. Phys. **89**, 6017 (1989)
11 V. Bulovic, V.B. Khalfin, G. Gu, P.E. Burrows, D.Z. Garbuzov, S.R. Forrest, Phys. Rev. B **58**, 3730 (1998)
12 K. Neyts, P.D. Visschere, D.K. Fork, G.B. Anderson, J. Opt. Soc. Am. B **17**, 14 (2000)
13 P.A. Hobson, J.A.E. Wasey, I. Sage, W.L. Barnes, IEEE J. Sel. Top. Quantum Electron. **8**, 378 (2002)